Journal of Applied Fluid Mechanics, Vol. 9, No. 5, pp. 2559-2568, 2016.
Available online at www.jafmonline.net, ISSN 1735-3572, EISSN 1735-3645.
DOI: 10.18869/acadpub.jafm.68.236.25086

Analysis of Rotor-Stator Interaction in Turbine Mode of a Pump-Turbine Model

D. Y. Li[1], R. Z. Gong[1], H. J. Wang[1†], X. Z. Wei[1, 2], Z. S. Liu[1] and D. Q. Qin[1, 2]

[1] *School of Energy Science and Engineering, Harbin Institute of Technology, Harbin, Heilongjiang, 150001, China*
[2] *State Key Laboratory of Hydro-Power Equipment, Harbin Institute of Large Electrical Machinery, Harbin, Heilongjiang, 150040, China*

†*Corresponding Author Email: wanghongjie@hit.edu.cn*

(Received May 18, 2015; accepted November 2, 2015)

ABSTRACT

The highest-level fluctuations in large pump-turbines are usually originated from rotor-stator interaction (RSI) in the vaneless region. Hence, the studies of RSI phenomenon and corresponding unsteady effects are significantly important to reduce the pressure fluctuations. In this paper, firstly, RSI in a pump-turbine, featuring 20 stay vanes, 20 guide vanes and 9 runner blades, is analyzed through diameter mode theory, which has been used widely. Then, 3-D unsteady numerical simulations are performed under six guide vane openings in turbine mode. The comparison including performance and pressure characteristics between numerical and experimental results shows a good agreement. Finally, best guide vane opening 21° is chosen to analyze the distribution of pressure fluctuations. The detailed investigation of numerical results shows that frequencies in the vaneless region at best guide vane opening are mainly blade passing frequency (BPF) and its harmonic frequencies caused from RSI. The variation of BPF and its harmonic frequencies is confirmed by diameter mode theory. For this type of the pump-turbine, the amplitude of 2BPF ($18f_n$) shows the highest corresponding diameter mode k_2=-2, which indicates two high pressure regions caused by the component of $18f_n$ in the vaneless region. Furthermore, the two high-pressure regions rotate in the counterclockwise direction with rotational speed of the runner blades. This research could provide a basic understanding of RSI to have a further study for pressure fluctuations in pump-turbines.

Keywords: Pump-turbine; Rotor-stator interaction; Turbine mode; Vaneless region; Diameter mode.

NOMENCLATURE

a	opening of the guide vanes	$\bar{p}$	time average calculation pressure
B_m	amplitude of the mth harmonic	T	torque of the runner
B_n	amplitude of the nth harmonic	T_B	rotational period of the blade
D_0	distribution diameter for guide vanes	y^+	non-dimensional wall distance
D_1	runner inlet diameter	Z_g	number of guide vanes
D_2	runner outlet diameter	Z_r	number of runner blades
f	frequency	Z_s	number of stay vanes
f_n	rotational frequency		
H	head of the pump-turbine	Φ_m	phase of the mth harmonic
m, n	harmonic order	Φ_n	phase of the nth harmonic
P_r	pressure field at runner inlet in rotating system	θ_r	angle coordinate in rotating system
		θ_s	angle coordinate in stationary system
P_s	pressure field at guide vane outlet in stationary system	ω	rotational speed
		η	hydraulic efficiency in turbine mode
p	calculation pressure		

1. INTRODUCTION

New green energies such as wind and solar, have a strong development during the last ten years, which lead to large fluctuations for the load of electrical power network since they are strongly dependent on meteorological conditions. In order to stabilize the electrical grid, a great number of hydropower plants

were developed due to their quick respond ability to the variation of the load (Decaix 2015), especially for pumped storage power plants. Because of effective storage and flexible switch between turbine mode and pump mode, pumped storage power plants have a rapid development. Pump-turbine as for the key component, the current trend is the increasing of the power, head, and speed either for building new plants or for upgrading existing plants. It leads to an obvious rise in the pressure and fluid velocities (Rodriguez 2007). A great number of studies were carried out on flow characteristics (Yin *et al.* 2010, 2014), instabilities such as hump characteristics (Li *et al.* 2015) and S shaped characteristics (Wang *et al.* 2011), and corresponding pressure fluctuations in pump-turbines. Pressure fluctuation is one of hot topics in pump-turbines. The increase of pressure fluctuations leads to the fatigue problems more common. Generally speaking, pressure fluctuations of pump-turbines in turbine mode operating at normal conditions for full load come from RSI. At part load they are mainly caused by the vortex rope in the draft tube cone. At extreme off-design operating condition, the pressure fluctuations are due to draft tube instabilities, runner channel vortices and flow separation (Magnoli 2012). These pressure fluctuations not only generate lot of noises and serious oscillations, but also introduce unfavorable characteristics. Hence, it is very important to understand the causes of pressure fluctuations to improve the overall performance and reliability (Wang *et al.* 2001).

RSI has specific characteristics that could be clearly observed in frequency and has been studied widely through different methods. Tanaka (1990), Guo and Marua (2005), Franke *et al.* (2005), and Guo and Okamoto (2014) have used excited diameter mode theory which was proposed by Kutota *et al.* (1983) to determine vibration characteristics combing the number of stationary and rotating blades. These studies could provide a quick and simple result. Meanwhile, lot of researchers predicted pressure fluctuation caused by RSI with a reasonable accuracy using CFD. Wang *et al.* (2001) predicted pressure fluctuations in 2-D unsteady incompressible flow by using a vortex method, which shows a good agreement with the experimental data. Yan (2010) obtained the pressure fluctuations in the vaneless region using a compressible CFD simulation and conducted that the compressibility of water might strongly influence the pressure fluctuation. Similar work was carried out by Yin (2013) to study the effects of water compressibility on pressure fluctuations. More recently, a conclusion was obtained that the rotating of guide vanes has an obvious effect on the amplitudes of pressure fluctuations in the vaneless region (Li 2015).

Although a great deal of research has been carried out to investigate pressure fluctuations, a systematic investigation of RSI in the vaneless region using numerical simulation, experimental validation and diameter mode theory is limited. The mechanism of RSI is not fully clear, especially for pump-turbines. In this paper, 3-D unsteady simulations of a pump-turbine, featuring 20 stay vanes, 20 guide vanes and 9 runner blades were conducted using the SST k-ω turbulence model in turbine mode. Based on the validation of the experimental data including performance and pressure characteristics, best guide vane opening 21° is selected to study the causes and propagation characteristics of RSI combing diameter mode theory in the vaneless region. In addition, the distribution of the pressure characteristics in the circumferential direction and vertical direction is also presented.

2. PUMP-TURBINE SPECIFICATIONS

A reversible pump-turbine model is investigated in this research, which is reduced 8 times of a prototype in a pump storage power plant (see Fig. 1). Main parameters of the pump-turbine in turbine mode are listed in Table 1. The five components are as follows: the spiral casing, the stay vanes, the guide vanes, the runner and draft tube. All the measurements are carried out on the hydraulic system in Harbin Institute of Large Electrical Machinery.

Fig. 1. The test rig of the pump-turbine model.

Table 1 Parameters of the pump-turbine model

Parameter	Value	Unit
D_1	482.5	mm
D_2	240	mm
Z_r	9	-
D_0	563.5	mm
Z_g	20	-
Z_s	20	-

3. EXPECTED ROTOR STATOR BEHAVIOR IN VANELESS REGION

Pressure filed caused by RSI in the vaneless region could be considered as a combination of inviscid flow (potential) and viscous flow (wake). With respect to potential effect, flow field in the vaneless region is periodically perturbed by the rotating runner blades. As for the viscous effect, the hydrodynamic phenomena, which play a major role in RSI, is non-uniformity of the velocity field in the spiral casing, non-desirable flow angle in the distributor, flow separations and wakes (Zobeiri, 2006).

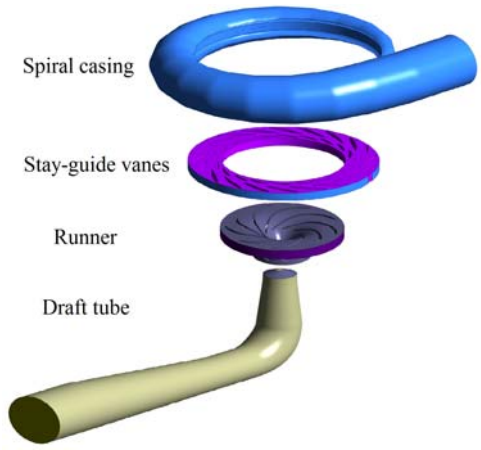

Fig. 2. Computational domain.

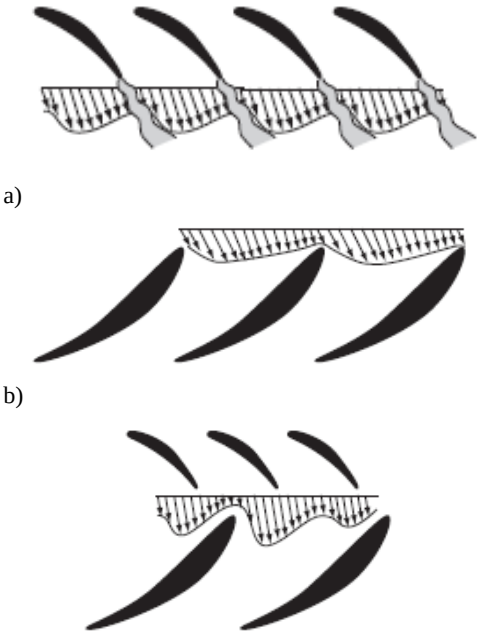

Fig. 3. Modulation process between the runner blade and guide vanes flow field a) flow field distortion due to guide vanes wakes, b) flow field distortion due to rotating runner blades, c) combination of both distortions (Zobeiri, 2006).

In the stationary system, the non-uniform flow field at the guide vane outlet is caused by wake effect. The loading of guide vanes creates a periodic flow field (see Fig. 3-a). In the rotating system, periodic flow field distortions are induced by the rotating runner blades (see Fig. 3-b). These stationary and rotating periodic flows can be expressed as the following Fourier series according to diameter mode number.

$$p_s\left(\theta_s,t\right)=\sum_{n=1}^{\infty}B_n\cos\left(n\cdot Z_g\cdot\theta_s+\phi_n\right) \tag{1}$$

$$p_r\left(\theta_r,t\right)=\sum_{m=1}^{\infty}B_m\cos\left(n\cdot Z_r\cdot\theta_r+\phi_m\right) \tag{2}$$

The final modulation can be expressed by Eq. (3) as the product of both pressure fields. Fig. 3 illustrates the modulation process between the rotating runner blades and guide vanes.

$$\begin{aligned}p_{mn}\left(\theta,t\right)=A_{mn}&\cos\left(n\cdot Z_g\cdot\theta_s+\phi_n\right)\\&\cdot\cos\left(m\cdot Z_r\cdot\theta_r+\phi_m\right)\end{aligned} \tag{3}$$

Using trigonometric identities in Eq. (3) and arranging the terms

$$\begin{aligned}p_{mn}\left(\theta_s,t\right)=&\frac{A_{mn}}{2}\cos\left(n\cdot Z_g\cdot\theta_s-m\cdot Z_r\cdot\theta_r+\phi_n-\phi_m\right)\\&+\frac{A_{mn}}{2}\cos\left(n\cdot Z_g\cdot\theta_s+m\cdot Z_r\cdot\theta_r+\phi_n+\phi_m\right)\end{aligned} \tag{4}$$

According to the relation of stationary system and rotating system, one can get the Eq. (5).

$$\theta_r=\theta_s-\omega t \tag{5}$$

Eq. (4) can be expressed as Eq. (6).

$$\begin{aligned}p_{mn}\left(\theta_s,t\right)=&\frac{A_{mn}}{2}\cos\left(mZ_r\omega\cdot t-\left(mZ_r-nZ_g\right)\theta_s+\phi_n-\phi_m\right)\\&+\frac{A_{mn}}{2}\cos\left(mZ_r\omega\cdot t-\left(mZ_r+nZ_g\right)\theta_s-\phi_n-\phi_m\right)\end{aligned} \tag{6}$$

Eq. (6) indicates the pressure fluctuation induced by potential interaction in the stationary system, which is the function of time and space. One defines two diameter modes k_1 and k_2, which can be expressed as Eq. (7) and Eq. (8).

$$k_1=m\cdot Z_r-n\cdot Z_g \tag{7}$$

$$k_2=m\cdot Z_r+n\cdot Z_g \tag{8}$$

Diameter mode k indicates the number of high-pressure regions and low-pressure regions for a frequency component in the circumferential direction, for example, $k=2$ means that there are two high-pressure regions and two low-pressure regions for one frequency component. Since the pressure field will be influenced by the rotating runner blades, the pressure distribution will change with the time, which will rotate in the same direction or opposite direction. The rotating speed is shown as Eq. (9) and Eq. (10).

$$\omega_1=m\cdot Z_r\cdot\omega/k_1 \tag{9}$$

$$\omega_2=m\cdot Z_r\cdot\omega/k_2 \tag{10}$$

Sign symbol decides the rotating direction. When k is positive, the direction is the same with the rotational direction of the runner, vice versa. In this research, the pump-turbine features 9 runner blades and 20 guide vanes. The expected rotor stator diametrical modes and corresponding to frequencies of the fluctuations are summarized in Table 2.

Table 2 Expected rotor stator diametrical modes and corresponding to fluctuation frequencies

n	m	k_1	k_2	ω_1/ω	ω_2/ω	$f/f_n=mZ_r$
1	**1**	**-11**	**29**	**-0.8**	**0.3**	**9**
1	**2**	**-2**	**38**	**-9.0**	**0.5**	**18**
1	3	7	47	3.9	0.6	27
1	4	16	56	2.3	0.6	36
1	5	25	65	1.8	0.7	45
2	1	-31	49	-0.3	0.2	9
2	2	-22	58	-0.8	0.3	18
2	3	-13	67	-2.1	0.4	27
2	**4**	**-4**	**76**	**-9.0**	**0.5**	**36**
2	**5**	**5**	**85**	**9.0**	**0.5**	**45**

According to other researchers' studies, the amplitude and power of pressure fluctuation is usually considered much lower if the harmonic order is higher. So only n=1, 2 are listed in Table 2. In Kubota's theory (1983), the absolute value of k shows higher, the amplitude of corresponding frequency is much lower, so k_2 is usually neglected. The absolute value k_1 is 2, while n=1 and m=1, corresponding frequency is $18f_n$ whose amplitude shows highest. In such case, the pressure field rotates in $9f_n$ in the opposite direction with the runner. Then the k_1 is -4, 5, 7, -11 and so on, the corresponding harmonic frequencies are marked in bold in the Table 1. It can be concluded that the main frequencies in the vaneless region caused by RSI are $9f_n$, $18f_n$, $27f_n$, $36f_n$, ⋯, which are mainly the blade passing frequency and its harmonic frequencies. The amplitudes of their main frequencies could be arranged by the value of k_1. Since the $36f_n$ and $45f_n$, are relatively high, one could neglect them in this analysis. As a consequence, the amplitudes of these main frequencies in a descending order are as following: $18f_n$, $27f_n$, $9f_n$, $36f_n$, $45f_n$, ⋯

In a sum, the frequencies and their amplitudes in the vaneless region are predicted through the theory, which need to be validated through numerical and experimental results in the following parts.

4. NUMERICAL SIMULATIONS

4.1 Mesh Generation

The commercial software ANSYS is employed in this research to create the mesh and carry out the simulations. Structured hexahedral meshes for the whole computational domain are created using ANSYS module ICEM. The computational domain is divided into five parts: spiral casing, stay vanes, guide vanes, runner and draft tube (see Fig. 4). The details of every components are summarized in Table 3. y^+ for stay vanes, guide vanes and runner in average is less than 2.

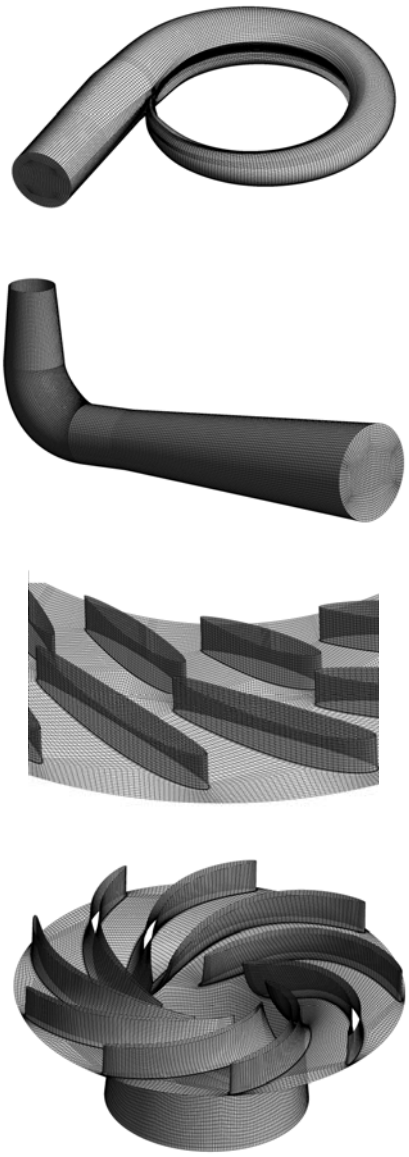

Fig. 4. Meshes for different components a) spiral casing, b) draft tube, c) guide-stay vanes, d) runner.

Table 3 Mesh details for different components

Component	Parameters	
	Nodes	y^+
Spiral casing	0.4	1488
Stay guide	0.7	1.82
Guide vanes	0.8	1.63
Runner	0.9	1.69
Draft tube	0.5	1408
Total (mil.)	3.4	

4.2 Boundary Conditions

The mass flow at spiral casing is used for the inlet boundary condition, which is set according to

experimental data. The turbulence parameters are specified in terms of turbulence intensity and hydraulic diameter of the inlet. Static pressure (0 Pa) is set at the draft tube outlet (turbine mode). Considering the recirculation and backflow, the type of pressure outlet is opening. In addition, smooth no-slip wall conditions are imposed for the rest of solid surfaces. Boundary function is adjusted to the low Reynolds number wall function. All the cases are investigated for the energy characteristics without considering the cavitation.

4.3 Numerical Scheme

All the simulations are conducted through ANSYS module CFX. 3-D incompressible unsteady Reynolds-averaged Naiver-stokes (URANS) equations and mass conservation equations are solved using finite volume method. Two-equation turbulence model SST k-ω is chosen for closing equations. In addition, the high resolution scheme is used for the advection term and 1st order upwind scheme is chosen for other terms. A time step 1.6×10^{-4}s is set corresponding 1.2° of runner rotation. Namely, a revolution for the runner needs 300 steps. The interface between rotor and stator is Transient Rotor-Stator.

4.4 Validation for Performance Characteristics

Six operation condition points of the pump-turbine in turbine mode for the identical rotational speed under different guide vane openings are chosen to validate the accuracy of the simulations. The variation of the head, torque and efficiency with guide vane opening is plotted in Fig. 5.

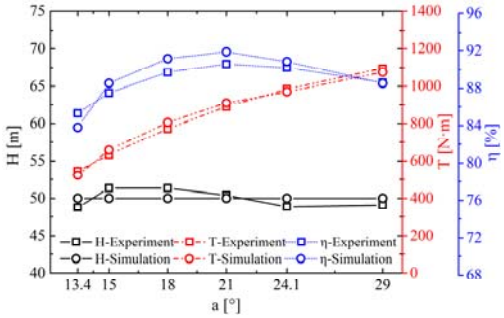

Fig. 5. Comparison for performance characteristics between the experiments and simulations.

From Fig. 5, the difference between experimental and numerical results for all performance characteristics curve is less than 5%. The maximal differences for the head, torque and efficiency between the experimental and numerical results are observed at 13.4° guide vane opening, which are -4.17%, -2.46% and -1.75%, respectively. The minimal differences appear at 29° guide vane opening. In a sum, the differences at large guide vane opening show less than the ones at small guide vane opening, and the relative differences turn out much larger off the best guide vane opening (21°).

The reasons for the differences between experimental and numerical results mainly come from the following. Firstly, 13.4° guide vane opening is small opening, which is an off-design operation condition, in which the flow pattern is extremely unstable and accompanies with flow separation, vortex motion and secondary flow. So the differences at this operation condition show the highest. Secondly, leakage and gap losses as well as dis friction are neglected in the usual CFD set up. Thirdly, the turbulence model based on URANS, which consists many empirical parameters, cannot predict all kinds of flow. In this research, SST k-ε turbulence model is chosen, and the differences for torque, head and efficiency are less 5%, 3% and 2%, respectively, which satisfy numerical accuracy. A further analysis could be carried out based on the validation above.

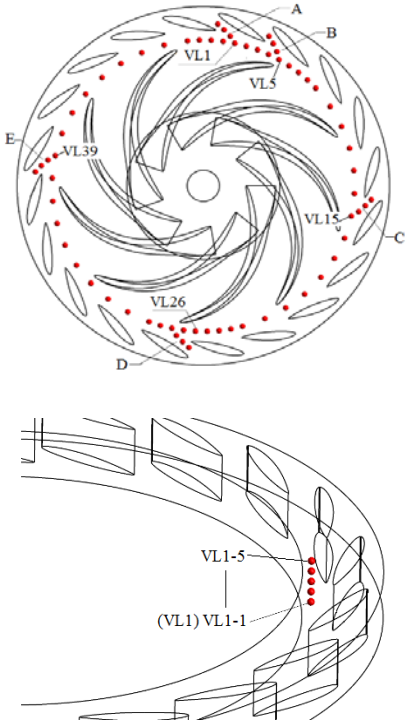

a)

b)

Fig. 6. Monitoring points in the vaneless region a) circumferential direction, b) vertical direction.

4.5 Validation for Pressure Fluctuations

Figure 6 shows the locations for monitoring points in the vaneless region. Fifty monitoring points are set in the vaneless region (between the runner inlet and guide vane outlet) close to the band (see Fig. 6-a) to investigate the pressure characteristics in the circumferential direction. Five (A, B, C, D and E) groups of monitoring points are set along the flow direction to investigate pressure characteristics in the flow direction. For each group, the distance of every two monitoring points is equal. All the monitoring points are equally copied four times in the vertical direction (see Fig. 6-b) to obtain the variation of pressure fluctuations in the vertical direction.

The calculation results of last 2048 steps are used to study the pressure characteristics compared with experimental data. The frequency resolution is 3Hz. Dimensionless parameter $\Delta H/H$ is used to represent how much the pressure fluctuation corresponding to relative head. ΔH is peak-to-peak value during the observing time. Point VL26 is an experimental and also a numerical monitoring point in the vaneless region. Fig. 7 gives the difference between the experimental and numerical results for point VL26.

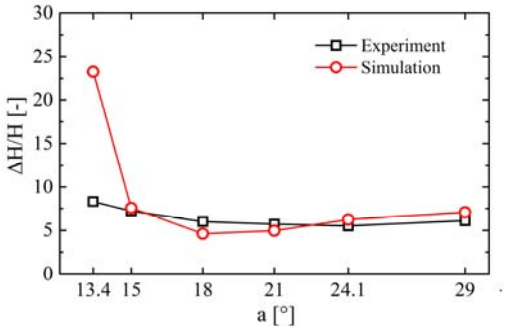

Fig. 7. Comparison for pressure fluctuation of experimental and numerical results.

From Fig. 7, it can be noticed that there is the same trend between the experiments and simulations. The minimal difference 13.3% is observed at best guide vane opening 21°. There appears a high difference at off design operation condition, whose maximal value reaches to 180.4%. In several studies (Magnoli and Schilling 2012; Xiao *et al.* 2008, 2010; Liu *et al.* 2012), the differences of $\Delta H/H$ between experiments and simulations also reach around 200% at the off-design operation conditions. The reasons for the differences mainly come from the following. Firstly, the compressibility of water and effects of fluid structure interaction (FSI) are neglected in the simulations. Secondly, peak-to-peak values might be not accuracy as the experimental results, since the sampling time during the simulations usually is less than the one for experiments due to the limited calculation resource and time.

5. NUMERICAL ANALYSIS IN VANELESS REGION

The non-dimensional coefficient of pressure fluctuation is defined in Eq. (11), which stands for how much the pressure fluctuations relative to the head. In this research, the head is 50 meters.

$$C_p = \frac{p - \overline{p}}{\rho g H} \times 100\% \tag{11}$$

21° best guide vane opening is chosen to simulate in order to investigate RSI without considering pressure fluctuations caused by other instabilities. The variation of $\Delta H/H$ for the five groups of monitoring points is shown in Fig. 8. It is found that the amplitudes of pressure fluctuations increase from the guide vane outlet to the runner inlet. For group A, the amplitude is 2.7% at the guide vane outlet, which increases to 6.7% at the runner inlet. The amplitudes close to the runner inlet show obviously higher than the ones at the guide vane outlet, which indicates the effects of RSI are the most serious close to the runner inlet.

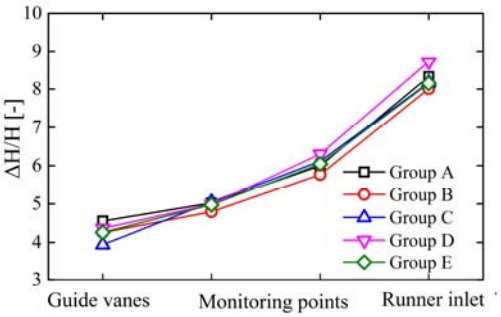

Fig. 8. Pressure fluctuation trend in the radial direction.

Figure 9 illustrates the variation in the vertical direction. The amplitudes close to the band (VL1-1) and the hub (VL1-5) are a bit higher than the ones in the other heights. The amplitudes in the different heights change little, the maximal difference is only 0.17% for group D. Hence, the monitoring points near the band and close to the runner inlet are chosen to investigate the pressure fluctuation characteristics.

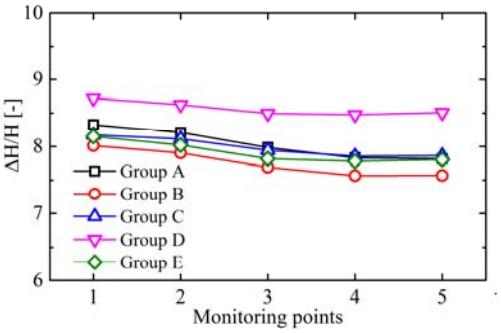

Fig. 9. Pressure fluctuation trend in the vertical direction.

The variation of $\Delta H/H$ in the circumferential direction is shown in Fig. 10. Abscissa represents the position at the circumference. The curve is generated through all the monitoring points in the clockwise direction, which features obviously periodic. In addition, the distance between two peaks (troughs) is 18°, which is the same as that of every two guide vanes. It indicates that pressure fluctuation appears a periodic variation passing every guide vane. All the monitoring points are marked in the vorticity field (see Fig. 11). The plane of vorticity field is chosen where all monitoring points are set. From the Fig. 11, it can be seen that the points which show a peak value are all located in guide vane wake regions. Guide vane wake regions usually consist wake space and momentum exchange space, which show strong shearing action with the main flow and high turbulent fluctuations. Composing the action of the rotating blades, the amplitudes of $\Delta H/H$ in guide vane wake regions show rather higher than the ones in other regions.

The wave trough points are located between the two guide vanes. The fluctuations mainly come from potential interaction, so the amplitudes are relatively low.

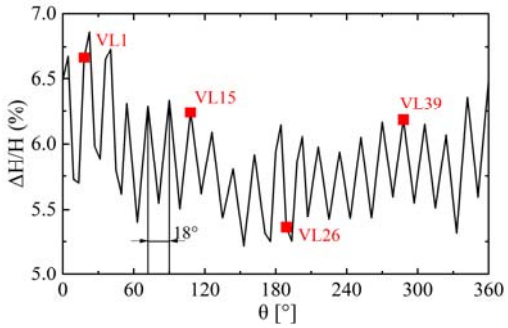

Fig. 10. Variation in the circumferential direction.

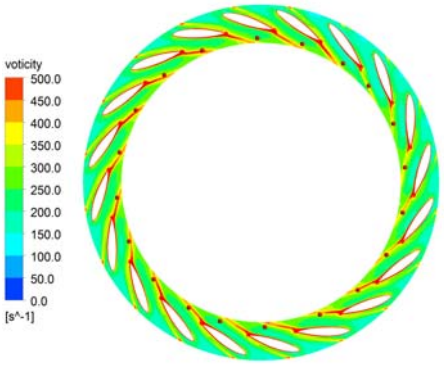

Fig. 11. Vorticity distribution in vaneless region.

In order to get the pressure characteristics in the circumferential direction, four points VL1, VL15, VL26 and VL39, are chosen to be analyzed using frequency spectrum and time domain methods. Fig. 12 shows pressure signals of different monitoring points in one runner revolution. From every picture, one can get the pressure fluctuation shows a periodic variation for all the monitoring points, The peak repeats every 5.28×10^{-3}s (rotational period of the blade). During this time, the runner rotates 40°. It indicates that the pressure fluctuations are obviously influenced by the rotating blades. Fig. 13 gives the pressure cloud chart of point VL1 at different moments, corresponding with the time marked in Fig. 12-a. Combining with contour of pressure, the pressure for the point VL1 is mainly influenced by pressure field caused by the head of the runner blade. Since the existing attacking angle in the head of the runner blades, one side will appear high-pressure region because of attacking while in another side there will appear low-pressure region due to flow separation. When $t_1=0T_B$, the pressure reaches to the peak, at this time, the monitoring point just locates in the high-pressure region. Then $t_2=0.18T_B$, the low-pressure region is close to monitoring point, which leads the pressure of the point to the lowest. As the runner continues to rotate, at $t_3=0.52T_B$ and $t_4=0.70T_B$, there are a small wave peak and a wave trough, respectively, which come from RSI between the guide vanes and the runner blades. RSI generates non-uniform pressure field. When to $t_4=1.00T_B$, at this moment there appears another wave peak, so variation of pressure fluctuation enters the next period.

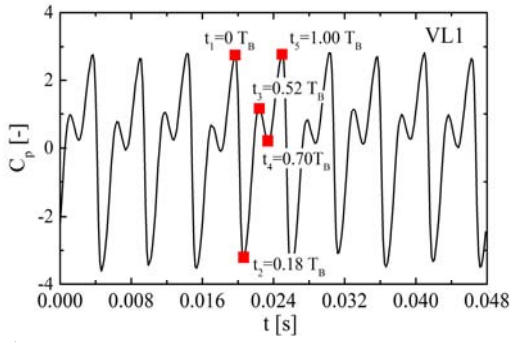

a)

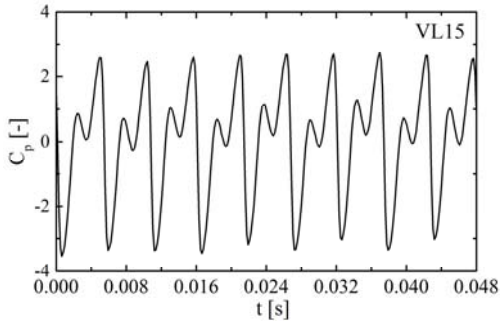

b)

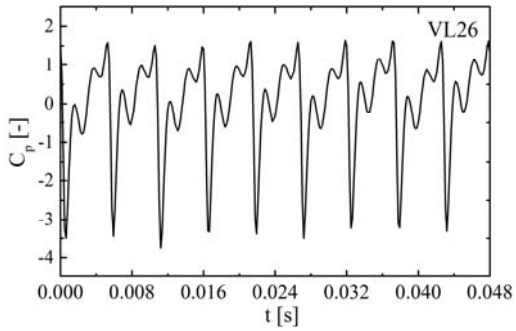

c)

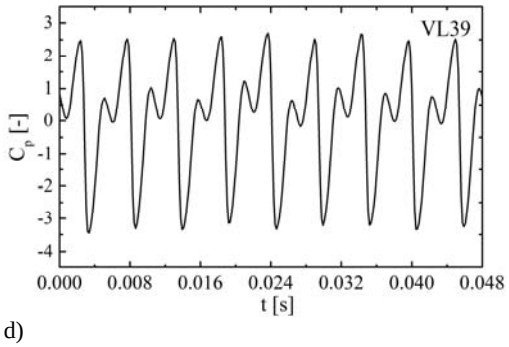

d)

Fig. 12. Pressure signals for different monitoring points a) VL1, b) VL15, c) VL26, d) VL39.

Excluding point VL26, pressure signals of the rest points have the same shape. The reason for this phenomena may be the result of different frequency components integrating. In addition, the signal phase shows very different among these four monitoring points, which directly shows pressure

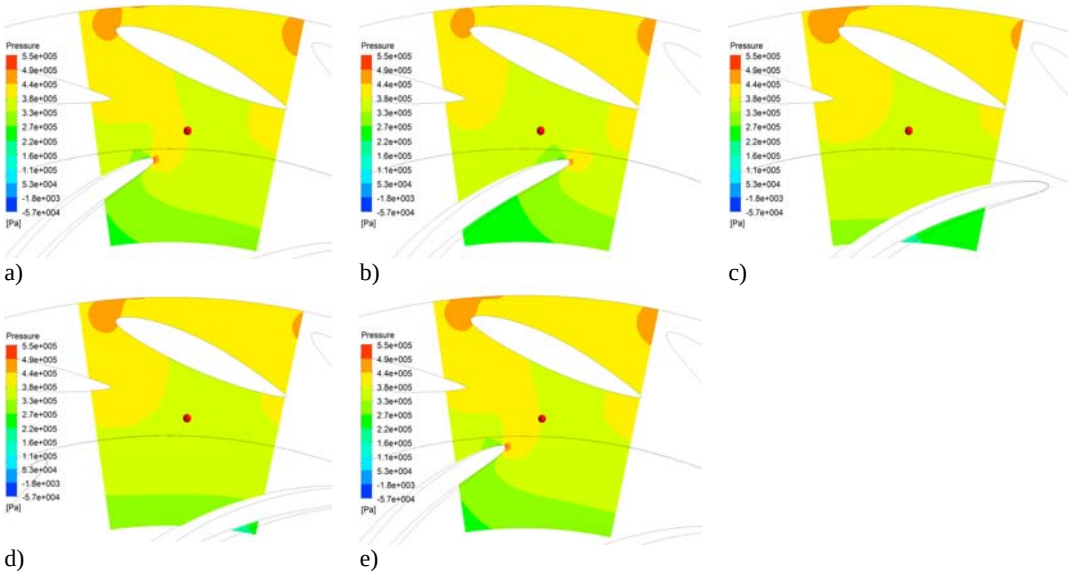

Fig. 13. Contour of pressure for point VL1 at different time a) t_1=0T_B, b) t_2=0.18T_B, c) t_3=0.52T_B, d) t_3=0.70T_B, e) t_4=1.00T_B.

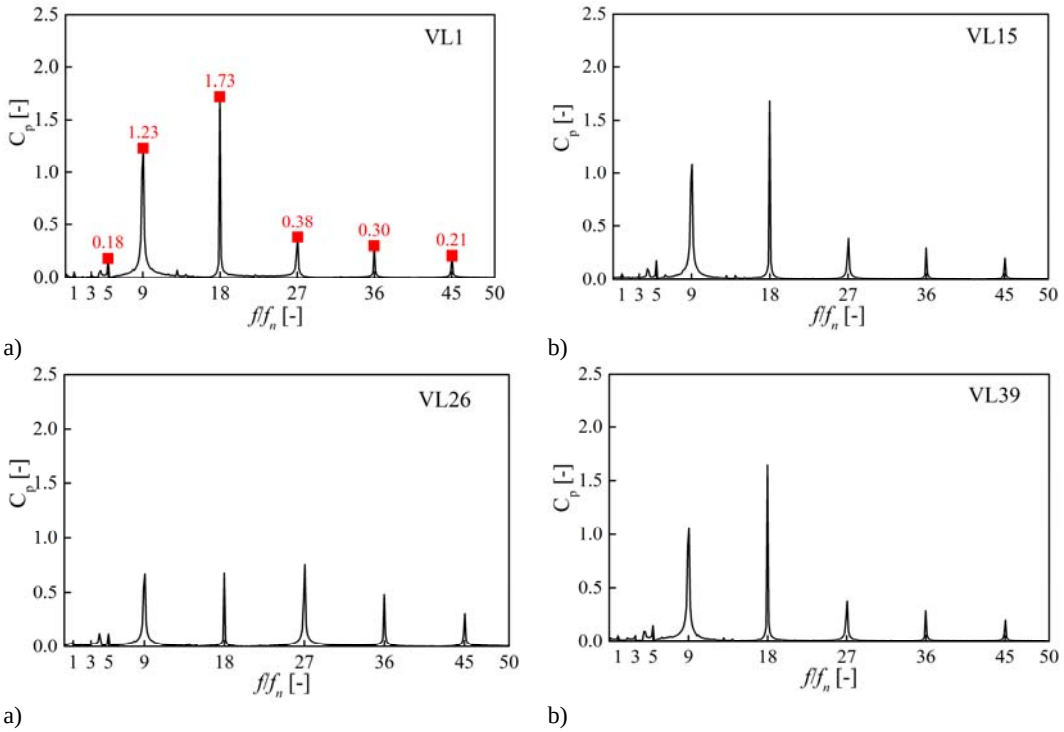

Fig. 14. Frequency spectrum for different monitoring points a) VL1, b) VL15, c) VL26, d) VL39.

wave propagation in the circumference.

Then, a Fourier analysis of all the pressure time data is performed to determine the prevailing frequencies at different locations (see Fig. 14). Where, f is real frequency, f_n is rotational frequency, 20.87Hz; frequency resolution is 0.146f_n.

It can be obtained that the main frequencies are blade passing frequency and its harmonic frequencies, such 9f_n, 18f_n, 27f_n, 36f_n, ⋯. So the frequencies in the vaneless region at best guide vane opening are originated potential interaction between the guide vanes and the runner blades. For point VL1, the first main frequency is 18f_n, with an amplitude of 1.73; the second main frequency is 9f_n, with an amplitude of 1.23. The amplitudes of 27f_n, 36f_n, and 45f_n, are relatively small and show a descending trend. This is the same with the results obtained through diameter mode theory.

However, the frequency characteristics of VL26 show different from the other three monitoring points. The amplitudes of 9f_n and 18f_n are much lower than those of other points, while the

amplitudes of 27f_n and 36f_n show relatively high. It indicates pressure field of different frequencies components features different distribution and wave propagation characteristics.

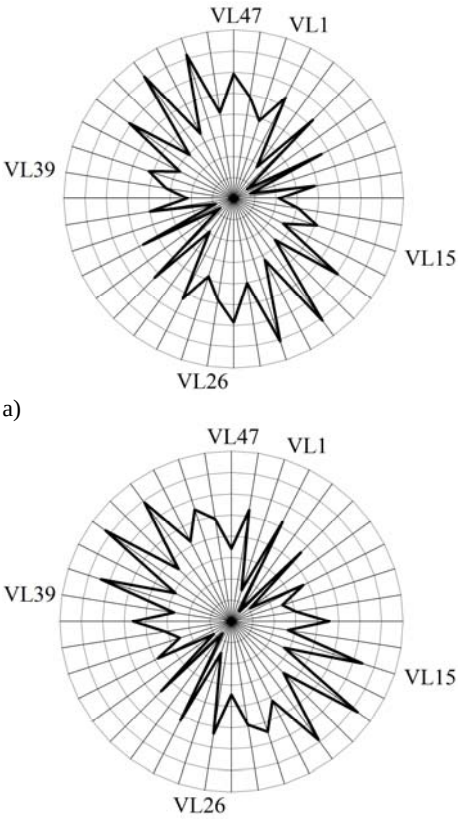

Fig. 15. Pressure field distribution of 18f_n at different moment a) 0.1s, b) 0.10032s.

In order to analyze the difference above, pressure time data is filtered to get the component of 18f_n. The time t_1=0.1s and t_2=0.10032s are chosen to get the radar map (see Fig. 15). Namely, from the moment t_1 to the moment t_2, the calculation continues 2 steps corresponding to 2.4° of the runner rotation. Both pictures show the pressure distribution exists two high-pressure regions and two low-pressure regions, which is the same with the results predicted through diameter mode theory, corresponding to k=-2 (18f_n). In addition, the pressure distribution rotates in counterclockwise direction with rotational speed of the runner blade (9ω). It can be concluded that pressure fluctuations in the vaneless region under the best guide vane opening of a pump-turbine in turbine mode, are mainly originated from RSI between the guide vanes and the runner blades. Frequencies are mainly blade passing frequency and its harmonic frequencies. Moreover, pressure distribution and propagation characteristics for the components of different frequencies could be confirmed through diameter mode theory.

In addition, excluding the blade passing frequency and its harmonic frequencies, there are still some low frequencies with small amplitudes, such as 0.15f_n, f_n, 4f_n, 5f_n. These frequencies are not produced by RSI and may come from other components, such as vortex motion, rope vortex in the draft tube. A further study could be continued to validate the sources of these frequency components.

6. CONCLUSION

A numerical investigation of a pump-turbine in turbine mode is carried out combining with the diameter mode theory. Numerical simulations are performed at six guide vane openings under identical rotational speed. Compared with the experimental results, a good agreement is demonstrated between them. The highest difference for head, torque and efficiency is less than 5%, 3% and 2%, respectively. With respect to pressure fluctuation $\Delta H/H$, there also shows the same trend between the experiment and simulations. The lowest difference is observed at the best guide vane opening of 21°. Based on the validation of the experiments, the variation of pressure fluctuations in the vaneless region is analyzed. Main frequencies are mainly blade passing frequency and its harmonic frequencies. Pressure fluctuations in the vaneless region at the best guide vane opening of a pump-turbine in turbine mode, are mainly originated from RSI between the guide vanes and the runner blades. The first and second main frequencies are 18f_n and 9f_n, respectively. Moreover, the pressure distribution of 18f_n rotates in the counterclockwise direction with rotational speed of the runner blade (9ω). Pressure distribution and propagation characteristics for the components of different frequencies are confirmed through diameter modes theory. Based on the analysis above, a further study should be continued to validate the sources of the low frequency components. When an emphasis on the other instabilities such as vortex rope, flow separation and secondary flow is carried out, effects caused by RSI could be filtered according to this study.

ACKNOWLEDGEMENTS

This work was supported by Foundation for Innovative Research Groups of the National Natural Science Foundation of China (Grant No. 51121004). The authors also would like to thank Harbin Institute of Large Electrical Machinery for its test platform for the experimental data of the pump-turbine.

REFERENCES

Berten, S., P. Dupont, M. Farhat and F. Avellan (2007). Rotor-stator interaction induced pressure fluctuations: CFD and hydroacoustic simulations in the stationary components of a multistage centrifugal pump, *Proceedings of FEDSM2007, 5th Joint ASME/JSME Fluids Engineering Conference*, San Diego, California USA 37549, 963-970.

Decaix, J., A. Mülle, F. Avellan and C. Münch (2015). Rans computations of a cavitating

vortex rope at full load. *6th IAHR International Meeting of the Workgroup on Cavitation and Dynamic Problems in Hydraulic Machinery and Systems*, Ljubljana, Slovenia.

Franke, G., R. Fisher, C. Powell, U. Seidel and J. Koutnik (2005). On pressure mode shapes arising from rotor stator interaction. *Sound and Vibration* 39(3), 14-18.

Guo, S. J. and H. Okamoto (2003). An experimental study on the fluid forces induced by rotor-stator interaction in a centrifugal pump. *International Journal of Rotating Machinery* 9(2), 135-144.

Guo, S. J. and Y. Maruta (2005). Experimental investigations on pressure fluctuations and vibration of the impeller in a centrifugal pump with vaned diffusers. *JSME International Journal Series B-Fluids and Thermal Engineering* 48(1), 136-143.

Kubota, Y., T. Suzuki, H. Tomita, T. Nagafugi and C. Okamura (1983). Vibration of rotating bladed disc excited by stationary distributed forces. *Bulletin of JSME* 26, 1952-1957.

Li, D. Y., H. J. Wang, G. M. Xiang, R. Z. Gong, X. Z. Wei and Z. S. Liu (2015). Unsteady simulation and analysis for hump characteristics of a pump turbine model. *Renewable Energy* 77, 32-42.

Li, D. Y., R. Z. Gong, H.J. Wang, G. M. Xiang, X. Z. Wei and Z. S. Liu (2015). Dynamic analysis on pressure fluctuation in vaneless region of a pump turbine. *SCIENCE CHINA Technological Sciences* 58, 813-824.

Liu, J. T., S. H. Liu, Y. L. Wu, L. Jiao, L. Q. Wang and Y. K. Sun (2012). Numerical investigation of the hump characteristic of a pump–turbine based on an improved cavitation model. *Computer and Fluids* 68, 105-111.

Magnoli, M. V., and R. Schilling (2012). Numerical simulation of pressure pulsations in Francis Turbines. *26th IAHR Symposium on Hydraulic Machinery and Systems*, Beijing, China 15(6), 062029. Tsinghua University.

Rodriguez, C. G., E. Egusquiza and I. F. Santos (2007). Frequencies in the vibration induced by the rotor stator interaction in a centrifugal pump turbine. *Journal of Fluids Engineering* 129, 1428-1435.

Shi, F. and H. Tsukamoto (2001). Numerical study of pressure fluctuations caused by impeller-diffuser interaction in a diffuser pump stage. *Journal of Fluids Engineering* 123, 466-474.

Tanaka, H. (2011). Vibration behavior and dynamic stress of runners of very high head reversible pump-turbines. *International Journal of Fluid Machinery and Systems* 4, 289-306.

Wang, H. and H. Tsukamoto (2001). Fundamental analysis on rotor-stator interaction in a diffuser pump by vortex method. *Journal of Fluids Engineering* 123, 737-747.

Wang, L. Q., J. L. Yin, L. Jiao, D. Z. Wu and D. Q. Qin. (2011). Numerical investigation in the "S" characteristics of a reduced pump turbine model. *SCIENCE CHINA Technological Sciences* 54, 1259-1266.

Xiao, Y., Z. Wang, Z. Yan, and J. Zhang (2010). Experimental and numerical analysis of pressure pulses characteristics in a Francis turbine with partial load. *IOP Conference Series-Earth and Environmental Science* 12, 012023.

Xiao, Y., Z. Wang, Z. Yan, Y. Luo, R. Xiao, G. Peng and P. Xue (2009). Experimental and numerical analysis of pressure pulsation in Francis turbine, *Proceedings of FEDSM2008, 2008 ASME Fluids Engineering Conference*, Jacksonville, Florida USA 55238, 1179-1185.

Yan, J., J. Koutnik, U. Seidel and B. Huebner (2010). Compressible simulation of rotor-stator interaction in pump-turbines. *IOP Conference Series: Earth and Environmental Science* 12, 012008.

Yin, J. L., D. Z. Wang, D. K. Walters and X. Z Wei (2014). Investigation of the unstable flow phenomenon in a pump turbine. *SCIENCE CHINA Physics, Mechanics and Astronomy* 57, 1119-1127.

Yin, J. L., D. Z. Wang, L. Q. Wang, Y. L. Wu and X. Z. Wei (2013). Effects of water compressibility on the pressure fluctuation prediction in pump turbine. *26th IAHR Symposium on Hydraulic Machinery and Systems*, Beijing, China, Tsinghua University.

Yin, J. L., J. T. Liu, L. Q. Wang, L. Jiao, D. Z. Wu and D. Q. Qin (2010). Performance prediction and flow analysis in the vaned distributor of a pump turbine under low flow rate in pump mode. *SCIENCE CHINA Technological Sciences* 53, 3302-3309.

Zobeiri, A., J. L. Kueny, M. Farhat and F. Avellan. (2006) Pump-turbine rotor-stator interactions in generating mode: Pressure fluctuation in distributor channel. *Proceedings of 23th IAHR Symposium on Hydraulic Machinery and Systems*, Yokohama, Japan 10, 1-10.